ROYAL SOCIETY
OF CHEMISTRY

PAPER

Check for updates

The degradation and recovery behavior of mixed-cation perovskite solar cells in moisture and a gas mixture environment†

George Wenson,[ab] Harshul Thakkar,[a] Hsinhan Tsai, [iD][a] Joshua Stein,[c] Rajinder Singh[a] and Wanyi Nie [iD] *[a]

Metal halide perovskites are not only established as champion materials for conversion of solar energy to electricity but are also one of the promising candidates for solar driven fuel generation. In this paper, we report the photovoltaic devices' operational stability investigation in dry and humid nitrogen (N_2) and carbon dioxide (CO_2) environments. By monitoring the behavior of a mixed-cation mixed-halide perovskite solar cell under constant 1-sun illumination in a gas mixture, we find that relative humidity plays a central role in expediting degradation. Interestingly, rapid degradation is a recoverable process once the light source is removed at the same humidity level. After a detailed analysis of the current–voltage characteristics, an increase in the series resistance is observed when exposed to continuous illumination. This is validated by surface resistivity measurements on both sides of the device. Photoluminescence (PL) characterization indicates a temporary decrease in the PL intensity and can be expedited by higher relative humidity levels. Our study reports behavior of perovskite solar cells in dry and wet N_2 and CO_2 environments that is necessary for solar-to-fuel applications like CO_2 reduction and water splitting in the gas phase.

Introduction

Industrial and research communities are working to find technologies that will enable them to reach 2030 greenhouse gas emission reduction targets.[1] Utilizing forms of renewable energy such as solar energy is one of the main strategies to address the climate crisis. There are many ways of converting solar energy into other forms; one popular application is solar fuel production *via* electrochemistry reactions. Such reactions require a high efficiency photo-catalyst to facilitate the reaction and the selectivity of the end product, which forms the core topic of the research community.

Halide perovskite semiconductors have been recently recognized as potential champion materials for optoelectronic applications such as photovoltaics and light-emitting diodes. The perovskite photovoltaic (PV) technologies have shown great promise in converting solar energy to electrical power. The field has made substantial progress in pushing power conversion efficiencies over 25% for cells[2–4] and extending the operational

lifetimes of perovskite PV that are required for commercialization. Alternate routes of utilizing perovskite materials for clean energy generation are being rigorously investigated. Notably, perovskite materials are being considered for driving photo-catalytic reactions especially for solar driven CO_2 reduction,[5–7] which can generate alternative fuels for energy while decarbonizing the environment. Perovskite nanocrystals with their tunable bandgap[8–12] and long carrier lifetimes[13–17] have been demonstrated as a promising photo-catalyst candidate to break stable C=O bonds, leading to the formation of hydrocarbons.[18–20] Very recently, perovskite solar cells have been used as an electron source to drive CO_2 reduction.[14,21–25] For all these applications, direct contact with water molecules or acid is required to lower the reaction barrier.[26–28] However, it is known that water can quickly degrade the perovskite layer upon contact, which will cause device failure.[26–29] For instance, the hydroscopic nature of the amine group in the cation salt of perovskite can cause its dissolution in water and revert the perovskite structure to the precursor phase. To circumvent this problem, Zhang *et al.* built an epoxy wrapped cell enclosure to extend the lifetime, and successfully demonstrated CO_2 reduction.[29] Others have explored non-aqueous environments, such as ionic liquid baths and polar aprotic solvent systems, that do not damage the perovskite materials for electrochemical reactions.[30,31]

While solving the stability problem is critical, it is also important to better understand the perovskite material

[a]*Los Alamos National Laboratory, 30 Bikini Atoll, Los Alamos, NM, 87545, USA. E-mail: wanyi@lanl.gov*

[b]*Honors College School of Engineering, Rutgers University, New Brunswick, NJ 008854, USA*

[c]*Sandia National Laboratory, Albuquerque, New Mexico, 87123, USA*

This journal is © The Royal Society of Chemistry 2022

J. Mater. Chem. A, 2022, **10**, 13519–13526 | **13519**

behaviors in a gas mixture of water and CO_2 or a nitrogen environment.[25,32–34] Perovskite solar cells are known to be sensitive to the moisture in the environment where the performance drops rapidly in the presence of high humidity. But uniquely, the devices can also self-heal once the light is removed.[35–37] The self-healing effect has been attributed to defect formation,[38] ion migration[35,36] and structural deformation.[39]

Recently, mixed-cation mixed-halide perovskites have been developed for high efficiency solar cells. The addition of ionic liquid has been proven to be a good strategy to stabilize the performance. But the cell stability of this system has not been investigated at various humidity levels. This is motivated by a recent study to investigate PSC device and photocatalysis operational stability under constant 1-sun illumination in various humidity/gas mixtures.[32,40] We observe a direct relation between the device's degradation rate and the relative humidity (R.H.) levels in the CO_2 gas. Interestingly, most of the performance loss can be restored when the light is turned off in the same R.H./CO_2 environment. By analyzing the current–voltage characteristics in greater detail, such as short circuit current density (J_{SC}), open circuit voltage (V_{OC}), and current–voltage curve slopes, we found that the series resistance of the cell increases upon illumination in a dry gas environment, and water molecules greatly advance such a change. The moisture assisted degradation is accompanied by a photoluminescence (PL) intensity drop. Our study concludes that R.H. has a direct impact on the cells' performance under constant illumination, and the performance losses can be restored in the same humid environment in the dark. These results are necessary when using the cells in a high humidity environment to drive reactions like CO_2 reduction or methane generation.

Experimental section

Materials

Lead(II) iodide (PbI_2, 99.999%), lead(II) bromide ($PbBr_2$, >98%), bathocuproine (BCP, 99.99%), formamidinium iodide (FAI, >99%), methylammonium iodide (MAI, >99%), cesium iodide (CsI, >99.9%), poly[bis(4-phenyl)(2,4,6-trimethylphenyl)amine], poly(triaryl amine) (PTAA, average M_n 7000–10 000), N,N-dimethylmethanamide (DMF, anhydrous, 99.8%), dimethyl sulfoxide (DMSO, anhydrous, >99.9%) and chlorobenzene (CB, anhydrous, 99.8%) were purchased from Sigma-Aldrich and used without further purification. [6,6]-Phenyl-C61-butyric acid methyl ester (C60-PCBM) was purchased from Nano-C and used as received.

Perovskite thin film and device fabrication

The perovskite photovoltaic has a device architecture of indium tin oxide (ITO)/PTAA/perovskites/PCBM/BCP/top electrode. The ITO substrates (7 Ω per square, Solaronix) were pre-cleaned and treated with ozone plasma before fabricating a hole transport layer. The PTAA solution (1 mg ml^{-1} in CB) was spun cast on an ITO substrate at 5k rpm for 30 s and then annealed at 100 °C for 20 minutes. The perovskite solution was made using 1.3 M of

($Cs_{0.05}FA_{0.8}MA_{0.2}PbI_{2.7}Br_{0.3}$) in DMF/DMSO (4 : 1) mix solution. The perovskite layers were prepared inside an argon-filled glovebox with a one-step antisolvent process. PCBM solution (20 mg ml^{-1} in CB) was spun cast on the perovskite layer at 4k rpm, followed by BCP (0.5 mg ml^{-1} in IPA) solution which was fabricated with 4k rpm. A 100 nm silver or gold layer was deposited on the final top electrode using thermal evaporation with a working area of 0.1 cm^2 defined by using a shadow mask under high vacuum (10^{-8} Torr).

Environmental chamber and illumination conditions

The perovskite devices were encased in an environmental chamber (reactor) and exposed to CO_2 with the relative humidity between 0 and 90% where the humidity was controlled by using a humidifier, as shown in Scheme 1. Scheme 1(a) shows the photoreactor system design and the actual system is shown in Scheme 1(b). The reactor was first purged with nitrogen (N_2) for 20 minutes to remove moisture, oxygen and other contaminants typically found in ambient air followed by dry and humid CO_2. To investigate the operation stability of these perovskite devices, a cyclic experiment (90 min with light-on/60 min dark) was carried out with CO_2/H_2O (50% R.H.) for a multiple cycle test.

Device stability test procedures

Once the perovskite devices were prepared, the product needed to be wired to form a working photovoltaic device. A glass slide was divided into two and the perovskite was attached with tape to the center of the half slide. Pieces of copper tape were placed on the glass slide on either side of the perovskite sample. A multimeter was used to identify which electrodes provided the greatest potential and pieces of copper tape were used to connect the gold electrodes to the copper tape on the side of the slide. These connections were overlayed with (Taiwan Carbon Materials Corp. X-CONDUCTOR™ Conductive Series (XD-R06)) silver paint to strengthen the connection between the electrode and the tape. On the positive terminal, silver paint was used to connect the copper tape to the ITO conductive glass underneath the perovskite layer. The potential of the solar cell would then be measured with a multimeter as a quality check to determine whether it functions or not. The devices underwent another
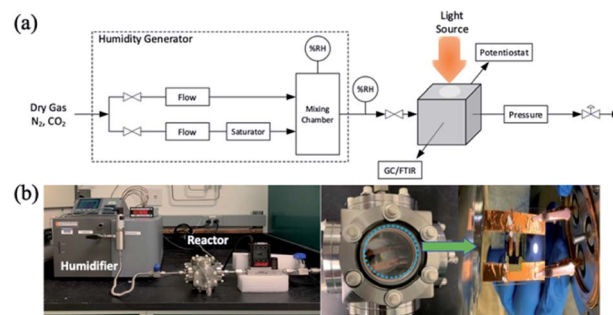
Scheme 1 (a) Photoreactor system design and (b) reactor system for perovskite devices.

round of quality control by performing preliminary current–density–voltage (J–V) curve measurements under ambient atmospheric conditions and 1-sun illumination (Class ABA solar simulator (Newport)). If the connections were done properly, then the J–V curves would yield clean data. Only after the devices passed these two tests, would they be allowed to go through to the data collection phase.

The devices were loaded into an environmental chamber with a window on the top side to let light into the apparatus. The chamber would be connected to a gas mixer as shown in Scheme 1(a) and (b), which would be used to control the humidity levels inside the environmental chamber. After the desired humidity level was reached, the environmental chamber would be wired to a Keithley 2400 source meter unit to measure the J–V curves for the device. The standard test would involve the environmental chamber being under constant illumination for two hours, after which the lamp would be turned off to observe the behavior of the cell in the dark. The sample would be re-illuminated only during the times when the J–V curve data were taken to ensure minimal amounts of degradation.

Results and discussion

Perovskite solar cell performance

The perovskite solar cell investigated in this work following an inverted p–i–n structure is shown in Fig. 1(a). Briefly, a pre-cleaned indium tin oxide (ITO) substrate is coated with a p-type polymer layer (poly[bis(4-phenyl)(2,4,6-trimethylphenyl]) amine, PTAA) as the hole transport layer (HTL). The perovskite absorbing layer is spin coated on the PTAA surface employing a popular mixed-cation, mixed-halide perovskite composition ($Cs_{0.05}FA_{0.75}MA_{0.2}PbI_{2.7}Br_{0.3}$) and is converted by an antisolvent approach.[16,41–45] The perovskite layer is processed

with ionic liquid as an additive in the precursor in order to suppress light-induced ion migration.[46,47] The n-type electron transport layer (ETL) is formed by spin coating a layer of phenyl-C_{61}-butyric acid methyl ester (PCBM) and a thin bathocuproine (BCP) layer on top of the perovskite. The device is completed by metallization with gold or silver. Here, silver was selected for efficiency characterization due to a better band alignment, and gold is selected for stability testing in gas environments to reduce the corrosion effect. The device dimensions are described in the experimental section. The device was first characterized by current–density–voltage (J–V) sweeps under 1-sun illumination.

Fig. 1(b) shows the J–V curves under dark and illuminated conditions. The dark and light J–V curves illustrate a typical diode behavior with the current on-off ratio of 4–7 orders of magnitude (Fig. S1 in ESI†) under the voltage range. In addition, forward and reverse voltage sweeps with a sweep rate of 10 mV s^{-1} are performed to test the hysteresis behavior in perovskite photovoltaics. Since the forward and reverse scans overlap well, the device in Fig. 1(c) is of high quality and free from hysteresis. The average power conversion efficiency (PCE) of the solar cells is 20.45 ± 0.32% with an open-circuit voltage (V_{OC}) of 1.09 ± 0.03 V, short-circuit current density (J_{SC}) of 23.56 ± 0.21 mA cm^{-2} and fill-factor (F.F.) of 79.84 ± 0.63%. The external quantum efficiency (EQE) is plotted and shown in Fig. 1(d) with the integrated photocurrent extracted from the EQE curve. The integrated current density (23.16 mA cm^{-2}) obtained from the EQE curve matches with the measured JSC from the J–V characteristic curves in Fig. 1(b) with less than 2% discrepancy. After confirming the device's performance, we then fabricated devices using the same processing conditions and replaced the top electrode with gold (Au). The Au devices were first characterized using dark J–V curves in air (Fig. S2†) and then transferred to a custom vacuum chamber (Fig. 1(e), also illustrated in Scheme 1 in the ESI†) outfitted with a quartz window and electrical feedthroughs. The vacuum chamber was initially pumped and purged with testing gas (N_2 or CO_2 with R.H. = x%, where x = 0, 20, 40, 60, 90) before data collection. The testing conditions in the dark and a 1-sun illumination environment are controlled by using a class ABA solar simulator with 1-sun equivalent intensity (100 mW cm^{-2}) after an air mass 1.5G filter.

Fig. 1 Photovoltaic device characterization and setup. (a) Device structure used in this study. (b) Typical dark (grey) and light (red) current–density–voltage curves; (c) light current–density–voltage characteristics when the voltage is swept from different polarities for the hysteresis behavior test. Both (b) and (c) are taken under a solar simulator with 1-sun intensity and a AM1.5G standard solar irradiation filter. (d) External quantum efficiency and the integrated short circuit current density taken under monochromatic light sources. (e) Gas environment setup used in this study. The device is mounted in a vacuum chamber, with the transparent electrode side facing the top quartz window where the light comes through.

Operational stability tests of the devices

Detailed summaries of the solar cell's responses to different gas mixture environments are shown in Fig. 2. Fig. 2(a)–(d) show the time evolution of the device's figures of merit, namely V_{OC}, J_{SC}, fill factor (F.F.) and power conversion efficiency (PCE), at different R.H. levels in CO_2 environments under constant illumination. The device's responses in dry nitrogen and dry CO_2 (repeat) air are also studied and shown in Fig. S3–S5 in the ESI.† By the end of a 2 hour constant illumination period, the V_{OC} drops by 5–15% when R.H. increases in the environment, whereas J_{SC} decreases by 40–60%. In both cases, a higher R.H. accelerates the degradation in the first 0–20 min testing period. The F.F. in Fig. 2(c) drops moderately by 10–20%, and R.H. also accelerates its degradation. Interestingly, in the 20–120 minute
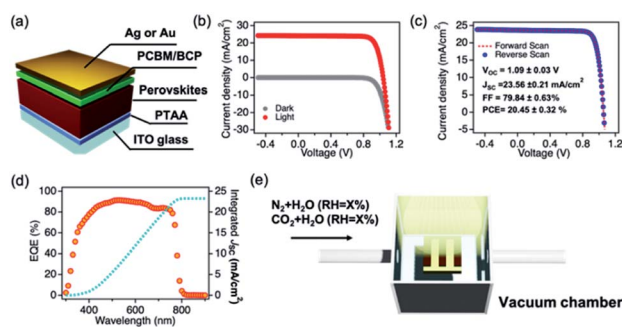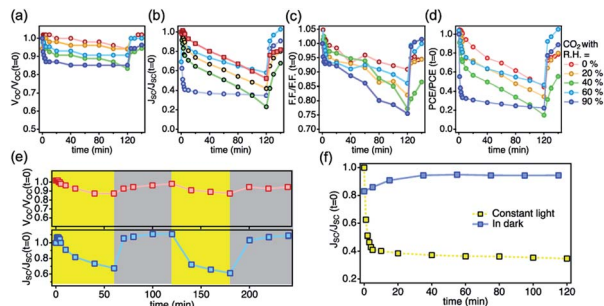
This journal is © The Royal Society of Chemistry 2022

J. Mater. Chem. A, 2022, **10**, 13519–13526 | **13521**

Fig. 2 Summary of the device stability results. Time evolution of the normalized (a) V_{OC}, (b) J_{SC}, (c) fill factor and (d) PCE at various R.H. levels and in CO_2 gas environments under constant illumination (0–120 min) and in the dark (120–140 min). (e) Time evolution of the device's normalized V_{OC} (upper panel) and J_{SC} (lower panel) under multiple light on (yellow region) and light off (grey region) cycles. (f) The time evolution of the normalized J_{SC} measured under constant illumination, and its recovery in 2 hours of darkness at 90% R.H.

Fig. 3 Detailed $J–V$ characteristic curve analysis. (a) Typical $J–V$ curves measured in the dark for a device being exposed to water/CO_2 with R.H. = 90% at fresh, degraded and recovered status. The dotted lines are the same data being plotted in a linear-log scale. The $J–V$ curves were measured by scanning from different bias polarities to observe the hysteresis. (b) The corresponding light $J–V$ curves and the normalized curves are shown in (c). Time evolution of the extracted normalized (d) R_{OC} values and (e) R_{SC} values for devices measured in dry CO_2 and humid CO_2 environments.

range, the degradation rates for V_{OC} and J_{SC} slow down and reach stabilized states only under high R.H. conditions. The overall PCE's degradation curve in Fig. 2(d) is determined by the J_{SC}, which loses its peak value most significantly. The raw $J–V$ curves are plotted and shown in Fig. S6–S8 in the ESI.† Also, light appears to be a vital element in the degradation of the solar cell. Fig. 2(a) and (b) show that when the device is no longer exposed to light, the normalized figures of merit are restored back to values close to the measurements at the beginning of the experiment. The device does not appear to be permanently damaged as can be seen in Fig. 2(e) within this testing period. To show reproducibility, we tested the devices under multiple light on/off cycles in an R.H. = 90% environment, and the difference in performance between cycles was minimal. Fig. 2(f) shows the healing effect of the device, which was tested at R.H. = 90% under dark and light cycling, and it is allowed to fully recover after being tested for 2 hours under the dark condition. This result shows how significant the light contribution is to the degradation of the solar cell. Also noticeably, at high R.H. = 90%, the device can recover its original performance within the testing period (*i.e.*, 120 min). Over longer-term exposure, the device's performance will ultimately drop (Fig. S12†) due to permanent damage to the perovskite materials as accepted by the established degradation mechanism.[48–50]

Fig. S11 in the ESI† compares the time evolution of the solar cell's figures of merit upon aging in dry N_2 and CO_2 gases under constant illumination. The device's degradation behaviors are very similar in both environments, indicating that CO_2 does not play a special role in the degradation behaviors.

Investigation of the solar cells' degradation mechanism

To gain a deeper insight into the degradation mechanism, a detailed analysis of the $J–V$ characteristics is carried out and the results are summarized in Fig. 3. The dark $J–V$ characteristics of a fresh device are compared in Fig. 3(a) after 1 hour illumination (degraded) and recovered in the dark after 100 min
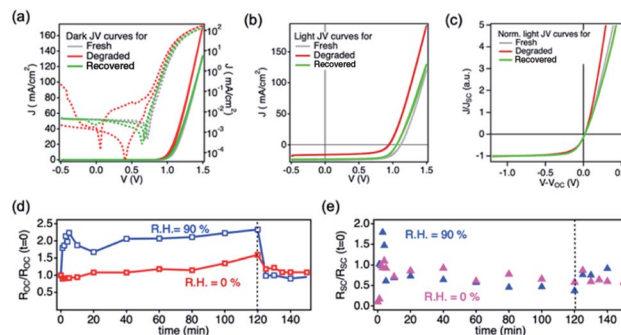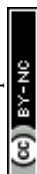
(recovered) under a CO_2/H_2O gas mixture environment with R.H. = 90%. The recovered curve (100 min) almost overlaps with the fresh curve, whereas the degraded device exhibits severe hysteresis (red dashed line). We have also checked perovskite films' crystallinity with the X-ray diffraction (XRD) patterns, and morphology *via* scanning electron microscopy (Fig. S9†) and UV-vis absorption (Fig. S10†) before and after gas exposure in ESI,† to confirm that the bulk composition remains unchanged within the testing period. In addition, the forward injection current increases for the degraded state which is reflected by the shift of the minimum point and the steeper slope at the forward bias.

Fig. 3(b) presents the device's $J–V$ curves under 1-sun illumination when it is in fresh, degraded and recovered states. To compare the slopes at the two fundamental points (*i.e.*, open-circuit (OC) and short-circuit (SC)), the normalized curves are shown in Fig. 3(c). It is clear that the slope does not change near the SC point for all conditions, whereas the slope changes more significantly near OC once the device is degraded, suggesting an increase in series resistance. This indicates that the humidity induced degradation mainly affects the current loss near the open circuit, which is related to the charge collection barrier near a low field. To compare the resistance at open circuit (R_{OC}) at all times when R.H. = 0% to 90%, Fig. 3(d) shows the time evolution of the normalized R_{OC} under constant illumination (0–120 min) and in the dark (120–150 min). Interestingly, the change in R_{OC} is concurrent with the light on/off cycles in both dry and humid environments. The high humidity level expedites the R_{OC}'s increase under illumination, and the R_{OC} drops back to the original value once light is removed which is similar to the device efficiency evolution shown in Fig. 2. In contrast, the time evolution of resistivity under the short circuit condition (R_{SC}) does not follow the light on/off cycles and is not affected by the relative humidity levels, as shown in Fig. 3(e). From these measurements, it is concluded that the R_{OC}'s increase accompanies the device degradation, and its rate is

13522 | *J. Mater. Chem. A*, 2022, **10**, 13519–13526

This journal is © The Royal Society of Chemistry 2022

also heavily impacted by the environmental conditions such as light and humidity whereas the R_{SC} is less affected.

To further understand the changes in electrical characteristics of the perovskite thin film when exposed to different gas environments, we examined the thin films' surface resistivity and photoluminescence changes under light and dark conditions. Fig. 4(a) shows two lateral device structures used for surface resistivity measurements. Here, we put two electrodes on the top of the perovskite/PCBM surface or deposit the perovskite on ITO with inter-digited patterns in order to probe the resistivity changes at the top and bottom interfaces respectively in moisture and light. Fig. 4(b) and (c) show the normalized resistivity evolution under one light–dark cycle in an R.H. = 90% environment. Interestingly, both resistivities measured at the top surface and bottom surface increase upon illumination in the R.H. = 90% condition and the values decrease to the original state once the light is off. These behaviors agree with the performance changes observed in Fig. 2, indicating that both interfaces are affected by illumination and humidity conditions. In addition, the increase in the surface resistivity values is consistent with the observation of the R_{OC} increase observed in Fig. 3, suggesting that insulating regions are formed when the light is on in a high humidity environment.

Furthermore, we performed PL stability tests under various relative humidity environments (R.H. = 0–60%) to deepen our understanding from a material perspective. Fig. 4(d) and (f) show the time evolution of the perovskite thin films' PL peak intensity (blue) and PL peak position (red) at R.H. = 0% and R.H. = 60% respectively. During the test period, the PL height remains unchanged at R.H. = 0% in each laser on/off cycle. In sharp contrast, once the R.H. increases to 60%, the PL height rapidly decreases upon laser irradiation, and can be restored to half the original value in the dark after multiple cycles. The peak positions, on the other hand, are not significantly affected by laser irradiation nor altered by R.H. values within the testing period. This is reflected in Fig. 4(e) and (g) where the PL spectra are plotted for R.H. = 0% and R.H. = 60%. In the mixed-cation, mixed-halide perovskite materials, light induced ion migration and phase segregation have been reported.[47,51] PL peak shifts or line shape changes are often employed to probe halide segregation. In this case, severe phase segregation induced PL line shape changes are not obvious even under a humid environment likely because of the addition of the ionic liquid that has been proven to be effective suppressing ion migrations.[46,47] Considering the resistivity changes shown in Fig. 4(b) and (c), the PL intensity drop can be attributed to the carrier scattering from the increased series resistance.

To briefly summarize the experimental observations, our study probes the perovskite solar cell's degradation behaviors in dry and humid CO_2 environments by using device characteristics in detail. For the solar cell's efficiency drop to be apparent in the short term, light-activation appears to be necessary. The degradation behavior at various humidities in Fig. 2 is only seen when the cell is exposed to light. However, while light does play an important role in the device's degradation, humidity also plays an essential role and should not be disregarded. The humidity of the environment coupled with the light condition determines how the device degrades; however, humidity alone does not provide the driving force to initiate the degradation process. The exposure to high humidity will ultimately damage the perovskite material as accepted by the research community. Here, our experiment probed only a short time period of device operation, that did not reach the time threshold for complete damage. Another interesting observation is that even though the J_{SC} drops much more than the V_{OC}, the J–V slope near SC is less affected when exposed to humidity with illumination. In all these processes, the moisture induced device degradations are temporary, $i.e.$, the device recovers once the light source is removed.

Literature studies have shown the chemical process of the perovskite degradation upon water exposure. The most common reaction route is the amine group in perovskites that can react with water and break the N–H–I hydrogen bonds resulting in the perovskite structure collapse.[52–55] Besides, grain boundaries are identified as the main sites where defect assisted degradation occurs. And the moisture can be adsorbed first near the grain boundary and initiating the material degradation.[56,57] This agrees with our findings that the resistivities of both the top and bottom surfaces change accordingly when the light is on, suggesting that light assisted moisture degradation occurs throughout the perovskite material, likely via the grain boundaries.

In our past investigation,[37] the light induced degradation and recovery effect was indeed observed in MAPbI$_3$ solar cells even in an inert gas environment. We have attributed such phenomena to the light induced charging effect (photo-charging) initiated near imperfections and interfaces. A
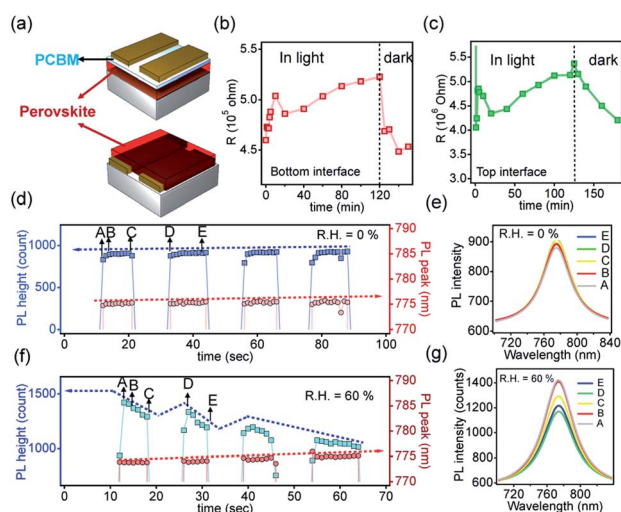

Fig. 4 Degradation mechanism investigations. (a) Schematic illustration of the device structures used for the lateral resistivity measurements; (b and c) the resistivity evolution under constant illumination and recovery in the dark where R.H. = 90% for both interfaces. Photoluminescence (PL) peak intensity and peak position for perovskite thin films (d) in 0% R.H. and (f) in 60% R.H. The corresponding PL spectra collected at various time points (A–E) are plotted in (e) and (g) respectively. The laser is CW 531 nm with a power density of 1 W cm^{-2}.

This journal is © The Royal Society of Chemistry 2022

J. Mater. Chem. A, 2022, **10**, 13519–13526 | **13523**

theoretical investigation[58] suggests that the photo-induced charging effect could also arise from the vacancy migration triggered by light. These mechanisms are associated with the defects in the perovskite layer.

In this current study, a similar light induced degradation and recovery was observed in dry N_2 and CO_2 environments, that could originate from the photo-charging mechanism. Here, the light induced charging effect alters the interface barrier which increases the R_{OC}, and promotes interface recombination that suppresses the V_{OC}. And this study reveals that increasing the R.H. levels in the environment accelerates degradation. Based on these observations, we think in a dry environment, the photo-charging effect degrades the performance initiated near the defect sites near grain boundaries and interfaces. And the presence of H_2O worsens the degradation rate. This also aligns with the observation of the PL intensity decreasing where more traps are available that capture the carriers.

It is suggested in the literature that the water molecule can be adsorbed on the surface or grain boundary *via* electro-static interactions, which in-turn dopes the surface. Water interacts electrostatically with a doped surface that can either fill the trap states[27,59] or donate electrons. A moisture induced surface doping effect or surface passivation effect largely depends on the perovskite's growth conditions,[60] where the initial surface of the perovskites can be either p-doped or n-doped. If the surface of the perovskite is n-doped, upon moisture exposure, the photoconductivity should increase due to the trap filling effect. On the other hand, if the surface is initially p-type, the moisture adsorption will neutralize the surface which decreases the photo-conductivity. Based on this mechanism, we think our perovskite surface is initially p-doped because of the iodine interstitial defect,[61] and the adsorption of moisture tends to neutralize the surface which increases the resistivity.

Such a mechanism can be borrowed in our mixed-cation mixed halide perovskite system, to explain the observed behavior of the increase of surface/bulk resistivity and R_{OC}. Interestingly, the recovery effect observed in our study suggests that such an adsorption is temporary and the removal of the light source can recover the device's performance even at high humidity levels.

Conclusions

In conclusion, our work probes the high performing mixed-cation, mixed halide perovskite solar cell's degradation and recovery behaviors in humid CO_2 environments. Our results indicate that constant illumination can degrade the cell's short circuit current and subsequently its efficiency; meanwhile, the presence of humidity greatly accelerates the degradation rate. Detailed device current–voltage characteristic analysis reveals that the series resistance of the device increases after degradation, whereas the shunt resistance remains unaffected. Backed up by the lateral resistivity and photoluminescence characterization studies, we conclude that the main mechanism for degradation can be attributed to the H_2O adsorption near the surface and grain boundaries forming an insulating phase that scatters the generated carriers. After these detailed studies, we

find that moisture plays a central role in device degradation whereas CO_2 behaves as non-reactive gas to the perovskite solar cells. Although the degradation gets more severe at high humidity levels, it is not permanent and the device can be restored in the dark. Our work validates that the mixed-cation mixed halide perovskite solar cell can work reasonably well in humid CO_2 environments, allowing for the high performing perovskite solar cell to function in those gas environments to drive photo-electro-chemistry reactions.
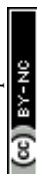
Conflicts of interest

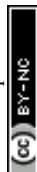The authors declare no competing interests.

Acknowledgements

References

1 T. W. House, *FACT SHEET: President Biden Sets 2030 Greenhouse Gas Pollution Reduction Target Aimed at Creating Good-Paying Union Jobs and Securing U.S. Leadership on Clean Energy Technologies*, https://www.whitehouse.gov/briefing-room/statements-releases/2021/04/22/fact-sheet-president-biden-sets-2030-greenhouse-gas-pollution-reduction-target-aimed-at-creating-good-paying-union-jobs-and-securing-u-s-leadership-on-clean-energy-technologies/, 2021.

2 J. J. Yoo, G. Seo, M. R. Chua, T. G. Park, Y. Lu, F. Rotermund, Y.-K. Kim, C. S. Moon, N. J. Jeon, J.-P. Correa-Baena, V. Bulović, S. S. Shin, M. G. Bawendi and J. Seo, *Nature*, 2021, **590**, 587–593.

3 J. Jeong, M. Kim, J. Seo, H. Lu, P. Ahlawat, A. Mishra, Y. Yang, M. A. Hope, F. T. Eickemeyer, M. Kim, Y. J. Yoon, I. W. Choi, B. P. Darwich, S. J. Choi, Y. Jo, J. H. Lee, B. Walker, S. M. Zakeeruddin, L. Emsley, U. Rothlisberger, A. Hagfeldt, D. S. Kim, M. Grätzel and J. Y. Kim, *Nature*, 2021, **592**, 381–385.

13524 | *J. Mater. Chem. A*, 2022, **10**, 13519–13526

This journal is © The Royal Society of Chemistry 2022

4 Y.-H. Lin, N. Sakai, P. Da, J. Wu, C. Sansom Harry, J. Ramadan Alexandra, S. Mahesh, J. Liu, D. J. Oliver Robert, J. Lim, L. Aspitarte, K. Sharma, P. K. Madhu, B. Morales-Vilches Anna, K. Nayak Pabitra, S. Bai, F. Gao, R. M. Grovenor Chris, B. Johnston Michael, G. Labram John, R. Durrant James, M. Ball James, B. Wenger, B. Stannowski and J. Snaith Henry, *Science*, 2020, **369**, 96–102.

5 N. Kato, S. Mizuno, M. Shiozawa, N. Nojiri, Y. Kawai, K. Fukumoto, T. Morikawa and Y. Takeda, *Joule*, 2021, **5**, 687–705.

6 J. He and C. Janáky, *ACS Energy Lett.*, 2020, **5**, 1996–2014.

7 W.-H. Cheng, M. H. Richter, I. Sullivan, D. M. Larson, C. Xiang, B. S. Brunschwig and H. A. Atwater, *ACS Energy Lett.*, 2020, **5**, 470–476.

8 H. Tsai, H.-H. Huang, J. Watt, C.-H. Hou, J. Strzalka, J.-J. Shyue, L. Wang and W. Nie, *Adv. Sci.*, 2022, 2105850.

9 H. Tsai, S. Shrestha, R. A. Vilá, W. Huang, C. Liu, C.-H. Hou, H.-H. Huang, X. Wen, M. Li, G. Wiederrecht, Y. Cui, M. Cotlet, X. Zhang, X. Ma and W. Nie, *Nat. Photonics*, 2021, **15**, 843–849.

10 Y. J. Yoon, K. T. Lee, T. K. Lee, S. H. Kim, Y. S. Shin, B. Walker, S. Y. Park, J. Heo, J. Lee, S. K. Kwak, G.-H. Kim and J. Y. Kim, *Joule*, 2018, **2**, 2105–2116.

11 Q. Chen, J. Wu, X. Ou, B. Huang, J. Almutlaq, A. A. Zhumekenov, X. Guan, S. Han, L. Liang, Z. Yi, J. Li, X. Xie, Y. Wang, Y. Li, D. Fan, D. B. L. Teh, A. H. All, O. F. Mohammed, O. M. Bakr, T. Wu, M. Bettinelli, H. Yang, W. Huang and X. Liu, *Nature*, 2018, **561**, 88–93.

12 L. Protesescu, S. Yakunin, M. I. Bodnarchuk, F. Krieg, R. Caputo, C. H. Hendon, R. X. Yang, A. Walsh and M. V. Kovalenko, *Nano Lett.*, 2015, **15**, 3692–3696.

13 S. Shrestha, X. Li, H. Tsai, C.-H. Hou, H.-H. Huang, D. Ghosh, J.-J. Shyue, L. Wang, S. Tretiak, X. Ma and W. Nie, *Chem*, 2022, **8**, 1107–1120.

14 Y. Jiang, C. Mei, Z. Zhang and Z. Dong, *Dalton Trans.*, 2021, **50**, 16711–16719.

15 C. M. M. Soe, C. C. Stoumpos, M. Kepenekian, B. Traoré, H. Tsai, W. Nie, B. Wang, C. Katan, R. Seshadri, A. D. Mohite, J. Even, T. J. Marks and M. G. Kanatzidis, *J. Am. Chem. Soc.*, 2017, **139**, 16297–16309.

16 M. Saliba, T. Matsui, K. Domanski, J.-Y. Seo, A. Ummadisingu, M. Zakeeruddin Shaik, J.-P. Correa-Baena, R. Tress Wolfgang, A. Abate, A. Hagfeldt and M. Grätzel, *Science*, 2016, **354**, 206–209.

17 D. Stranks Samuel, E. Eperon Giles, G. Grancini, C. Menelaou, J. P. Alcocer Marcelo, T. Leijtens, M. Herz Laura, A. Petrozza and J. Snaith Henry, *Science*, 2013, **342**, 341–344.

18 M. C. O. Monteiro, F. Dattila, B. Hagedoorn, R. García-Muelas, N. López and M. T. M. Koper, *Nat. Catal.*, 2021, **4**, 654–662.

19 H. Xu, D. Rebollar, H. He, L. Chong, Y. Liu, C. Liu, C.-J. Sun, T. Li, J. V. Muntean, R. E. Winans, D.-J. Liu and T. Xu, *Nat. Energy*, 2020, **5**, 623–632.

20 J. S. Derrick, M. Loipersberger, R. Chatterjee, D. A. Iovan, P. T. Smith, K. Chakarawet, J. Yano, J. R. Long, M. Head-Gordon and C. J. Chang, *J. Am. Chem. Soc.*, 2020, **142**, 20489–20501.

21 S. Shyamal and N. Pradhan, *J. Phys. Chem. Lett.*, 2020, **11**, 6921–6934.

22 H. Huang, B. Pradhan, J. Hofkens, M. B. J. Roeffaers and J. A. Steele, *ACS Energy Lett.*, 2020, **5**, 1107–1123.

23 Z. Chen, Y. Hu, J. Wang, Q. Shen, Y. Zhang, C. Ding, Y. Bai, G. Jiang, Z. Li and N. Gaponik, *Chem. Mater.*, 2020, **32**, 1517–1525.

24 A. Pan, X. Ma, S. Huang, Y. Wu, M. Jia, Y. Shi, Y. Liu, P. Wangyang, L. He and Y. Liu, *J. Phys. Chem. Lett.*, 2019, **10**, 6590–6597.

25 Y.-F. Xu, M.-Z. Yang, B.-X. Chen, X.-D. Wang, H.-Y. Chen, D.-B. Kuang and C.-Y. Su, *J. Am. Chem. Soc.*, 2017, **139**, 5660–5663.

26 J. Yang, B. D. Siempelkamp, D. Liu and T. L. Kelly, *ACS Nano*, 2015, **9**, 1955–1963.

27 A. M. A. Leguy, Y. Hu, M. Campoy-Quiles, M. I. Alonso, O. J. Weber, P. Azarhoosh, M. van Schilfgaarde, M. T. Weller, T. Bein, J. Nelson, P. Docampo and P. R. F. Barnes, *Chem. Mater.*, 2015, **27**, 3397–3407.

28 G. Niu, W. Li, F. Meng, L. Wang, H. Dong and Y. Qiu, *J. Mater. Chem. A*, 2014, **2**, 705–710.

29 H. Zhang, Y. Chen, H. Wang, H. Wang, W. Ma, X. Zong and C. Li, *Adv. Energy Mater.*, 2020, **10**, 2002105.

30 G. F. Samu, R. A. Scheidt, P. V. Kamat and C. Janáky, *Chem. Mater.*, 2018, **30**, 561–569.

31 M. Hasan, S. Venkatesan, D. Lyashenko, J. D. Slinker and A. Zakhidov, *Anal. Chem.*, 2017, **89**, 9649–9653.

32 J. Kong, Y. Shin, J. A. Röhr, H. Wang, J. Meng, Y. Wu, A. Katzenberg, G. Kim, D. Y. Kim, T.-D. Li, E. Chau, F. Antonio, T. Siboonruang, S. Kwon, K. Lee, J. R. Kim, M. A. Modestino, H. Wang and A. D. Taylor, *Nature*, 2021, **594**, 51–56.

33 S. S. Bhosale, A. K. Kharade, E. Jokar, A. Fathi, S.-m. Chang and E. W.-G. Diau, *J. Am. Chem. Soc.*, 2019, **141**, 20434–20442.

34 M. Ou, W. Tu, S. Yin, W. Xing, S. Wu, H. Wang, S. Wan, Q. Zhong and R. Xu, *Angew. Chem., Int. Ed.*, 2018, **57**, 13570–13574.

35 K. Domanski, B. Roose, T. Matsui, M. Saliba, S.-H. Turren-Cruz, J.-P. Correa-Baena, C. R. Carmona, G. Richardson, J. M. Foster, F. De Angelis, J. M. Ball, A. Petrozza, N. Mine, M. K. Nazeeruddin, W. Tress, M. Grätzel, U. Steiner, A. Hagfeldt and A. Abate, *Energy Environ. Sci.*, 2017, **10**, 604–613.

36 Y. Zhao, J. Wei, H. Li, Y. Yan, W. Zhou, D. Yu and Q. Zhao, *Nat. Commun.*, 2016, **7**, 10228.

37 W. Nie, J.-C. Blancon, A. J. Neukirch, K. Appavoo, H. Tsai, M. Chhowalla, M. A. Alam, M. Y. Sfeir, C. Katan, J. Even, S. Tretiak, J. J. Crochet, G. Gupta and A. D. Mohite, *Nat. Commun.*, 2016, **7**, 11574.

38 G. Nan, X. Zhang and G. Lu, *J. Phys. Chem. Lett.*, 2019, **10**, 7774–7780.

39 A. J. Neukirch, W. Nie, J.-C. Blancon, K. Appavoo, H. Tsai, M. Y. Sfeir, C. Katan, L. Pedesseau, J. Even, J. J. Crochet,

This journal is © The Royal Society of Chemistry 2022

J. Mater. Chem. A, 2022, **10**, 13519–13526 | **13525**

G. Gupta, A. D. Mohite and S. Tretiak, *Nano Lett.*, 2016, **16**, 3809–3816.

40 L. Shi, P. Bucknall Martin, L. Young Trevor, M. Zhang, L. Hu, J. Bing, S. Lee Da, J. Kim, T. Wu, N. Takamure, R. McKenzie David, S. Huang, A. Green Martin and W. Y. Ho-Baillie Anita, *Science*, 2020, **368**, eaba2412.

41 H.-H. Huang, H. Tsai, R. Raja, S.-L. Lin, D. Ghosh, C.-H. Hou, J.-J. Shyue, S. Tretiak, W. Chen, K.-F. Lin, W. Nie and L. Wang, *ACS Energy Lett.*, 2021, **6**, 3376–3385.

42 H.-H. Huang, Q.-H. Liu, H. Tsai, S. Shrestha, L.-Y. Su, P.-T. Chen, Y.-T. Chen, T.-A. Yang, H. Lu, C.-H. Chuang, K.-F. Lin, S.-P. Rwei, W. Nie and L. Wang, *Joule*, 2021, **5**, 958–974.

43 M. Degani, Q. An, M. Albaladejo-Siguan, J. Hofstetter Yvonne, C. Cho, F. Paulus, G. Grancini and Y. Vaynzof, *Sci. Adv.*, 2021, **7**, eabj7930.

44 M. Saliba, T. Matsui, J.-Y. Seo, K. Domanski, J.-P. Correa-Baena, M. K. Nazeeruddin, S. M. Zakeeruddin, W. Tress, A. Abate, A. Hagfeldt and M. Grätzel, *Energy Environ. Sci.*, 2016, **9**, 1989–1997.

45 D. Bi, W. Tress, M. I. Dar, P. Gao, J. Luo, C. Renevier, K. Schenk, A. Abate, F. Giordano, J.-P. Correa Baena, J.-D. Decoppet, M. Zakeeruddin Shaik, K. Nazeeruddin Mohammad, M. Grätzel and A. Hagfeldt, *Sci. Adv.*, 2016, **2**, e1501170.

46 T. Niu, L. Chao, W. Gao, C. Ran, L. Song, Y. Chen, L. Fu and W. Huang, *ACS Energy Lett.*, 2021, **6**, 1453–1479.

47 S. Bai, P. Da, C. Li, Z. Wang, Z. Yuan, F. Fu, M. Kawecki, X. Liu, N. Sakai, J. T.-W. Wang, S. Huettner, S. Buecheler, M. Fahlman, F. Gao and H. J. Snaith, *Nature*, 2019, **571**, 245–250.

48 P. Guo, Q. Ye, C. Liu, F. Cao, X. Yang, L. Ye, W. Zhao, H. Wang, L. Li and H. Wang, *Adv. Funct. Mater.*, 2020, **30**, 2002639.

49 Q. Wang, B. Chen, Y. Liu, Y. Deng, Y. Bai, Q. Dong and J. Huang, *Energy Environ. Sci.*, 2017, **10**, 516–522.

50 N. Aristidou, C. Eames, I. Sanchez-Molina, X. Bu, J. Kosco, M. S. Islam and S. A. Haque, *Nat. Commun.*, 2017, **8**, 15218.

51 M. Abdi-Jalebi, Z. Andaji-Garmaroudi, S. Cacovich, C. Stavrakas, B. Philippe, J. M. Richter, M. Alsari, E. P. Booker, E. M. Hutter, A. J. Pearson, S. Lilliu, T. J. Savenije, H. Rensmo, G. Divitini, C. Ducati, R. H. Friend and S. D. Stranks, *Nature*, 2018, **555**, 497–501.

52 M. Kim, A. Alfano, G. Perotto, M. Serri, N. Dengo, A. Mezzetti, S. Gross, M. Prato, M. Salerno, A. Rizzo, R. Sorrentino, E. Cescon, G. Meneghesso, F. Di Fonzo, A. Petrozza, T. Gatti and F. Lamberti, *Commun. Mater.*, 2021, **2**, 6.

53 R. T. Wang, A. F. Xu, J. Y. Chen, L. W. Yang, G. Xu, V. Jarvis and J. F. Britten, *J. Phys. Chem. Lett.*, 2019, **10**, 7245–7250.

54 Y. Li, W. Zhou, Y. Li, W. Huang, Z. Zhang, G. Chen, H. Wang, G.-H. Wu, N. Rolston, R. Vila, W. Chiu and Y. Cui, *Joule*, 2019, **3**, 2854–2866.

55 J. S. Yun, J. Kim, T. Young, R. J. Patterson, D. Kim, J. Seidel, S. Lim, M. A. Green, S. Huang and A. Ho-Baillie, *Adv. Funct. Mater.*, 2018, **28**, 1705363.

56 E. Ochoa-Martinez, M. Ochoa, R. D. Ortuso, P. Ferdowsi, R. Carron, A. N. Tiwari, U. Steiner and M. Saliba, *ACS Energy Lett.*, 2021, **6**, 2626–2634.

57 N. Phung, A. Al-Ashouri, S. Meloni, A. Mattoni, S. Albrecht, E. L. Unger, A. Merdasa and A. Abate, *Adv. Energy Mater.*, 2020, **10**, 1903735.

58 H. Shahivandi, M. Vaezzadeh and M. Saeidi, *Sol. Energy Mater. Sol. Cells*, 2020, **208**, 110383.

59 J. Huang, S. Tan, P. D. Lund and H. Zhou, *Energy Environ. Sci.*, 2017, **10**, 2284–2311.

60 M. A. Haque, A. Syed, F. H. Akhtar, R. Shevate, S. Singh, K.-V. Peinemann, D. Baran and T. Wu, *ACS Appl. Mater. Interfaces*, 2019, **11**, 29821–29829.

61 S. Shrestha, H. Tsai, M. Yoho, D. Ghosh, F. Liu, Y. Lei, J. Tisdale, J. Baldwin, S. Xu, A. J. Neukirch, S. Tretiak, D. Vo and W. Nie, *ACS Appl. Mater. Interfaces*, 2020, **12**, 45533–45540.

13526 | *J. Mater. Chem. A*, 2022, **10**, 13519–13526

This journal is © The Royal Society of Chemistry 2022